Toward Taper-Free Structures in Ultrashort Pulse Laser Ablation Using Liquid Crystal Spatial Light Modulators

Martin Osbild*[1], Mario Hesker[2], Moritz Battermann[1], Gang Lu[1], and Dennis Haasler[1]

[1]*Fraunhofer Institute for Laser Technology ILT, Germany*
[2]*RWTH Aachen Univ., Chair for Technology of Optical Systems TOS, Germany*
[*]*Corresponding author's e-mail: martin.osbild@ilt.fraunhofer.de*

Conventional ultrashort pulse laser microstructuring or cutting is inherently prone to the generation of tapered walls. This effect can only be compensated for by means of a defined manipulation of the angle of incidence (AOI) of the focused beam. This study explores the feasibility of using liquid crystal on silicon spatial light modulators (SLM) to achieve vertical wall angles in laser ablation. In the proposed method, the raw beam is passed sequentially over two cascaded SLMs to create a parallel offset that results in an altered AOI on the workpiece. This offers capabilities beyond established solutions such as simultaneous beam splitting and shaping. In a first step, investigations on laser cutting of stainless steel sheets are carried out to analyze the wall angle as a function of the most influencing parameters. Results indicate a minimum AOI of 3° is essential for taper-free structures, which is respected in the optics design considerations for the double-SLM module. Furthermore, the trade-off between optical efficiency and beam path length is quantitatively presented. Finally, recommendations for selecting the focal length of the f-theta lens and the scanning system are provided based on analytical calculations and optical simulations.
DOI: 10.2961/jlmn.2025.01.2003
Keywords: ultrashort pulse, laser ablation, SLM, angle of incidence, taper-free structures

1. Introduction

Ultrashort pulse (USP) laser processing offers several significant advantages over mechanical micro-milling techniques. USP lasers generally provide higher precision and operate without wear, eliminating the need for frequent tool replacement and thereby reducing maintenance costs.

Despite these strengths, USP laser ablation typically produces tapered walls in structuring, drilling or cutting operations unlike mechanical milling. Oftentimes, the targeted functionality is negatively affected or completely hindered by tapered walls. This phenomenon arises because a USP laser pulse exhibits a higher energy density in the center of the Gaussian beam, gradually decreasing toward the edges. This non-uniformity results in more pronounced ablation in the central region and leaves behind an inclined crater wall. Tophat profiles are not exempt from this effect as the steepness of intensity at the edges of the profile is also diffraction-limited and therefore exhibits a gradient. Subsequent laser pulses encounter an inclined wall, which influences both the absorptance and the incident energy density.

As established by Fresnel's laws, the degree of absorptance is a function of the angle of incidence (AOI, depicted in Fig. 1) and the polarization of the light. For p-polarized light, the absorptance increases with increasing AOI up to the Brewster angle, which for metals is typically in the range of 70 to 80 degrees [1]. Beyond this angle, the absorptance generally declines until it reaches zero when the AOI is 90°, which means that the beam propagates parallelly to the wall surface. For s-polarized light, the absorption decreases monotonically with increasing AOI. Circularly polarized light, being a combination of s- and p-polarized components, exhibits absorptance behavior that is intermediate between the two, without extreme variations.

The second effect, which occurs when a laser pulse strikes an inclined wall, is the enlargement of the illuminated area. Since the pulse energy typically remains constant, the enlarged illuminated area lowers the effective peak fluence $F_{0,\mathrm{eff}}$ which is given by the equation

$$F_{0,eff} = F_0 \cdot \cos\theta \,, \tag{1}$$

where F_0 is the peak fluence of a single pulse and θ is the AOI. This effect is the dominating one, leading to a decrease in absorbed effective fluence from pulse to pulse regardless of the polarization state [2].

With each additional laser pulse, the wall is removed slightly more so that the illuminated area increases until the effective fluence falls below the ablation threshold, resulting in a stable asymptotic wall angle that no longer changes with additional pulses [3].

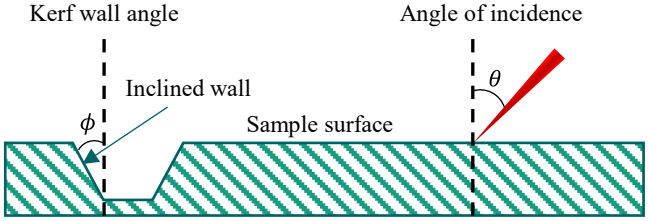

Fig. 1 The wall angle ϕ is defined as the mean angle between the generated structure wall and the initial surface normal. The AOI θ is defined as the angle between the laser ray and the local surface normal.

Vertical wall angles are frequently demanded for various applications and can only be achieved using an inclined laser beam. There is a multitude of commercially available technical solutions that solve the problem of inclined walls during drilling. With these processing heads for helical drilling or trepanning, the inclined laser beam rotates continuously in a precession movement around the optical axis. The material ejection is supported by a coaxial process gas nozzle [4-8]. Such a process is considerably limited in the applicable pulse repetition rate and can only be extended to a cutting process by means of slow workpiece movement. For cutting or structuring with fast beam deflection via galvo scanners, on the other hand, there are fewer solutions with which the beam can be inclined. These systems use additional galvo-controlled mirrors to offset the input beam parallelly in front of the galvo scanner [9, 10].

The aim of this study is to investigate whether vertical wall angles can also be achieved by using two liquid crystal on silicon spatial light modulators (simply abbreviated with SLM in the following) placed in front of the galvo scanner to induce a parallel offset. SLMs are becoming increasingly attractive for high-throughput material processing as they can withstand more and more average laser power, recent developments claiming to withstand over 700 W [11]. In addition, they offer the possibility of superimposed beam shaping and splitting, which makes them more versatile for a range of tasks. Particularly the possibility of simultaneous beam splitting can significantly reduce the process time for laser cutting of straight lines compared to helical cutting.

In a first step, fundamental investigations on scanner-based USP cutting of stainless steel sheets are carried out. These findings are then employed to assess the viability of an optical system for beam tilting based on SLM technology.

2. Investigations on the wall angle

The following section presents a series of parameter studies conducted under normal laser beam incidence. The objective of these studies is to gain insights into the correlation between the process parameters and the cutting result, with a particular focus on the kerf wall angle.

2.1 Experimental setup

The material samples used in the experimental investigations are stainless steel (AISI420) sheets with a thickness of 300 µm. The threshold fluence of this material was determined to be F_{thr} = (107.8 ± 1.2) mJ/cm² after saturation of the incubation effect.

The machining system is equipped with a USP laser beam source from EDGEWAVE, which emits laser radiation with a wavelength of 1030 nm, a pulse duration of 800 fs and a maximum average power of 70 W. A quarter waveplate is used to transform the initially linear laser radiation into a circularly polarized beam. The galvanometer scanner utilized is the IntelliSCAN III 14 from SCANLAB.

The expanded raw beam is focused using an f-theta lens with a focal length of 125 mm, resulting in a focal diameter ($1/e^2$) of 26 µm. The focus position is set on the sample surface, as this is a favorable position for a minimal wall angle [12].

Rectangular structures with a length of 3 mm and a width of 0.3 mm are created by a bidirectional hatching process with scan vectors aligned parallelly to the long side of the rectangle. The track overlap defined by the hatching distance and laser spot size amounts to 75%. The pulse overlap is also set to 75%, meaning that an increase in the pulse repetition rate leads to a proportional adjustment of the scanning speed. The total number of pulses per pass remain constant The varied process parameters are listed in Table 1.

Table 1 Varied process parameters

Peak fluence F_0	0.75 – 10 J/cm²
Number of passes N	20 – 5000
Repetition rate f_{rep}	10 – 500 kHz

After laser cutting, the stainless steel sheets are mechanically cut perpendicularly to the scanning direction in the center of the machined kerfs and embedded in resin in an upright orientation. The embedded samples are then ground and polished to obtain a flat and burr-free surface for examination. Finally, the cross-sectional profiles are imaged with a high-resolution light microscope which allows for a precise analysis of the kerf wall angles.

2.2 Experimental results

In a preliminary experiment, a repetition rate of f_{rep} = 10 kHz was determined to be the limit before heat accumulating between two subsequent pulses occurs. This repetition rate was selected and kept constant for the first series of experiments, while the other variables F_0 and N were varied. A selection of the resulting cross-sectional microscope images is shown in Fig. 2. The experiments demonstrated an overall good cut quality across all studied fluences. The walls seem to exhibit a smooth surface. However, pronounced grooves appear at the edges, which are due to side wall reflections starting at approximately 10 times the threshold fluence F_{thr}. Furthermore, at fluences exceeding 4 J/cm², pronounced roughness peaks can be observed in the cross-sectional view of the ablated bottom.

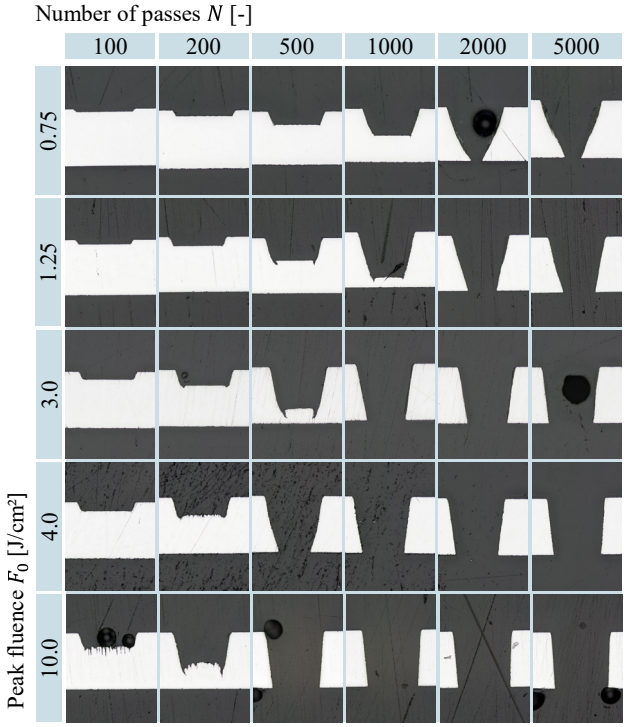

Fig. 2 Microscope images of selected cutting kerf cross-sections generated with a constant repetition rate of 10 kHz.

Fig. 3 shows the evolution of the measured wall angles over 3 orders of magnitudes of passes for different fluences. As expected, the wall angle decreases with increasing fluence and number of passes. One can observe a saturation effect as the wall angle does not change anymore with more passes which is known as asymptotic wall angle [3]. The smallest achievable wall angle in this experiment is 3° which is in accordance to the literature [Braunschweig2018]. It is achieved with a fluence of F_0 = 10 J/cm² and 5000 passes. Further significant reduction of the wall angle is not to be expected without increasing the fluence drastically. Experiments conducted at a higher repetition rate up to 500 kHz did not reveal a significant change in the wall angles. It leaves the question open if heat accumulation has only a minor effect on the wall angle or if the chosen upper repetition rate was still too low to show any significant effect.

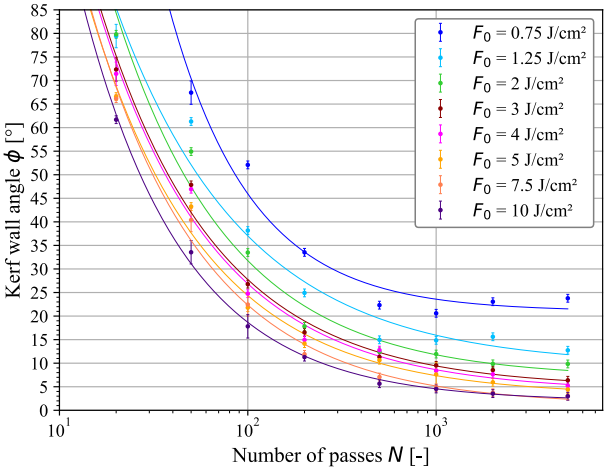

Fig. 3 Kerf wall angle as a function of the number of passes for different fluences at 10 kHz. The fitting curves follow the function $f(x) = A \cdot x^B + C$ as presented in [3]. The data points are weighted by log(N) for the fitting. An asymptotic behaviour is observed.

From the series of experiments, it can be concluded that an SLM-based beam manipulation system must achieve an AOI of at least 3°. However, an AOI of 5° or more would be much more desirable as significantly fewer passes would be required for a taper-free ablation result.

3. SLM-based manipulation of the AOI

In the following, the potential for digital control of the AOI using two cascaded SLMs is evaluated and discussed alongside with other hardware aspects of the optics design.

3.1 Basic principles

An SLM consists of a layer of liquid crystals deposited on a reflective silicon chip. The silicon chip acts as an active matrix that uses electrical voltage to control the orientation of the liquid crystal molecules. This allows the local refractive index to be set pixel by pixel. The partial beams of an incident laser pulse are individually retarded in phase, whereby after reflection at the SLM according to Huygens' principle, they collectively contribute to the manipulation of the laser pulse's characteristics. This capability enables precise control over beam splitting, shaping, and propagation direction. Furthermore, a combination of these can be performed by the pixel-wise phase modulation. Beam deflection at an SLM, which is essential for the AOI manipulation, can be compared to diffraction at a digital blazed grating. A blazed grating is a type of optical grating specifically designed to direct light into a preferred diffraction order. The diffraction angle induced by the grating depends on the wavelength of the light λ and the grating period, which is, for an LCoS-SLM, the product of the number of pixels p and the pixel pitch a. The first order diffraction angle which is the same as the deflection angle α follows the equation for the first-order diffraction angle at a grating

$$\sin\alpha = \frac{\lambda}{p \cdot a} \quad (2)$$

For beam shaping of splitting using the Gerchberg-Saxton algorithm, a superposed blazed grating phase mask is often applied for separating the shaped beam (1st order diffraction) from the undiffracted beam (0th order diffraction) [13]. The shorter the grating period, the larger the deflection angle, but at cost of the efficiency due to larger phase jumps between adjacent pixels leading to more distributed energy into other diffraction orders. In the worst cases, the quality of the deflected beam even deteriorates when the grating period is too short [13]. Fig. 4 shows the basic principle of beam deflection at an SLM and illustrates the effects stemming from different grating periods.

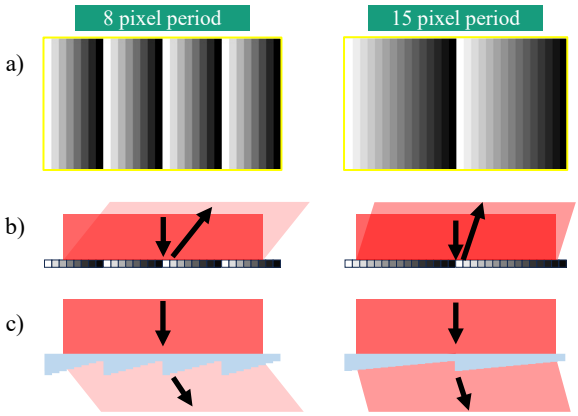

Fig. 4 Illustration of the working principle of beam deflection at an SLM for two different pixel periods. a) The phase mask 8 bit grayscale bitmap in 2D. b) The deflection at the SLM. c) The analogy to a transmissive blazed grating whose surface is discretized according to the pixels. Note that the color intensity of the deflected beam shows the efficiency qualitatively.

To be able to manipulate the AOI, the input beam must have a certain parallel offset with regard to the optical axis when entering the scanner. We present a method using two cascaded SLMs to create this parallel offset which is illustrated in Fig. 5. The first SLM displays a blazed grating phase mask, making the beam propagate an angle of α with regard to the optical axis. To parallelize the beam again, a second SLM must be placed in the beam path displaying the same blazed grating phase mask but mirrored. The longer the beam path is between the two SLMs, the larger is the resulting parallel offset Δd of the raw beam which is approximately proportional to the AOI θ. That also means that a long distance between the two SLMs is advantageous because one can use longer grating periods resulting in higher

optical efficiencies. The relationship between parallel offset Δd at a paraxial focusing lens and the AOI θ is given by

$$\tan\theta = \frac{\Delta d}{f}, \tag{3}$$

with the focal length f. It is obvious that a short focal length is advantageous because it leads to larger AOIs or requires smaller parallel offsets Δd, respectively. The latter also involves less constraints due to apertures along the beam path including the entrance pupil of the f-theta lens allowing for longer scan vectors. In addition, higher optical efficiencies are achieved at smaller parallel offsets and thus smaller required diffraction angles when the distance between both SLMs is fixed.

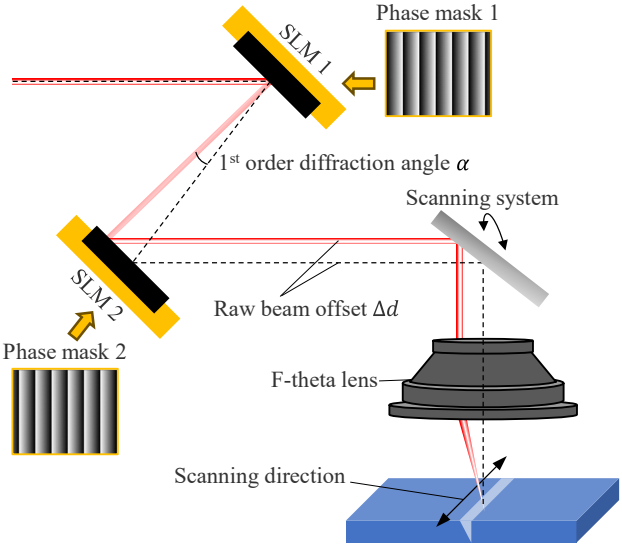

Fig. 5 Schematic of manipulation of the AOI in a scanning laser process by means of a parallel raw beam offset induced by two cascaded SLMs with blazed grating phase masks.

In the ideal paraxial case according to Eq. 3, the AOI of 3°, which we defined as minimum, would be achieved with a raw beam offset of Δd = 2.6 mm when using a focal length of f = 50 mm. A target AOI of 5° would require an offset of Δd = 4.4 mm.

3.2 Optical efficiency

An SLM from Hamamatsu Photonics' X15213 series was used for the following experiment. This is a typical SLM used for beam manipulation tasks in laser material processing, especially in research. Another, but similar laser beam source from Edgewave providing 1030 nm and 1.5 ps was used. Intensity measurements were conducted using a CMOS camera, with the baseline intensity I_0 determined without any grating phase mask. A thermal power meter would not be suitable for this tasks as it cannot distinguish between different diffraction orders. The SLM has a pixel pitch of p = 12.5 µm. The period of the blazed grating as shown in Fig. 4 was varied from 8 to 50 pixels. The intensity of the diffracted spot of the 1st order was measured and normalized with regard to I_0. The diffraction angle is given by the equation (2) and calculated for the different grating periods. The results are plotted in Fig. 6.

It was observed that the second-order diffraction spot is too pronounced when the grating period a is set to ≤9. Thus, the shortest acceptable grating period is 10 pixels in this setup which leads to a diffraction angle of 0.47° while only yielding a diffraction efficiency of 15%. Please note that in case for a parallel raw beam offset using two SLMs, the optical efficiency is squared. Therefore, a decent total efficiency of >50%, for example, would be met in case of a grating period of 20 pixels at the cost of a smaller diffraction angle (0.24°) and thus a longer required beam path between the two SLMs. For a target offset of Δd = 2.6 mm (for AOI = 3 @f = 50 mm), one would need a distance between the two SLMs of 0.6 m which can already be challenging for a limited spatial capacity. A target offset of Δd = 4.4 mm (for AOI = 5 @f = 50 mm) would already require a distance of 1.1 m

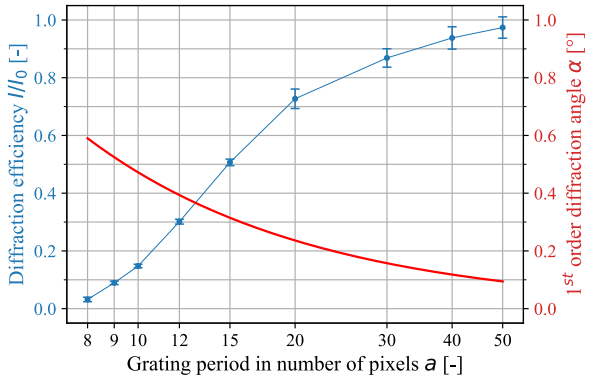

Fig. 6 Measured diffraction efficiency and calculated diffraction angles for different blazed grating configurations for one SLM. Five images per configuration were acquired, post-processed and the fitted intensity peaks averaged with a standard deviation. The x-axis is logarithmically scaled.

A total optical efficiency of >75% could be achieved with 30 pixels as grating period. It would require a distance of 0.9 m and 1.6 m between the two SLMs, respectively, depending on the target AOI of 3° or 5°. It becomes obvious that the available space is one of the essential limiting factors when developing an SLM-based optics module for the manipulation of the AOI.

3.3 AOI stability during scanning

Conventional 2-mirror galvo scanners are most commonly used in laser micro processing applications due to their high precision and speed. These systems consist of two mirrors, each controlled by a galvanometer motor. While these scanners combined with f-theta lenses are highly effective for various tasks, they inherently suffer from a telecentric error that can disturb the target AOI.

In a perfectly telecentric system, the beam always hits the workpiece orthogonally, regardless of its position in the scan field. However, in conventional 2-mirror systems, the pivot point refers to the virtual point around which the laser beam appears to rotate when deflected by the two mirrors. It is located between both mirrors. In reality, every beam deflection operation automatically leads to a beam offset from the pivot point resulting in a typically small tilt of the focused beam known as telecentric error that cannot be suppressed. The telecentric error is position-dependent and becomes more pronounced the farther the focus spot is

displaced from the scan field center. The superposition of the telecentric error with the intendedly manipulated AOI would yield unstable wall angles as ablation result.

An alternative scanner concept for laser material processing is the use of a single mirror 2-axis scanner. Recently, models with deflection angles of up to 240 mrad have become available, such as the Newson Cyclops system [14]. It offers a compact alternative to conventional 2-axis scanners, whereby the pivot point is fixed at one point on the mirror surface. This property is supposed to guarantee a minimized telecentric error. Whether this also facilitates the robustness of beam inclination will be investigated in detail in the following.

The optical simulations for this study were executed in Zemax OpticsStudio with several key assumptions and parameters to ensure accurate and reliable results. A typical raw beam diameter of 3 mm (1/e²) is chosen. To mitigate diffraction effects at any apertures, we applied a safety margin of factor 2 on the beam size. An ideal 50 mm f-theta lens was utilized in the simulation as it is a commonly used short focal length.

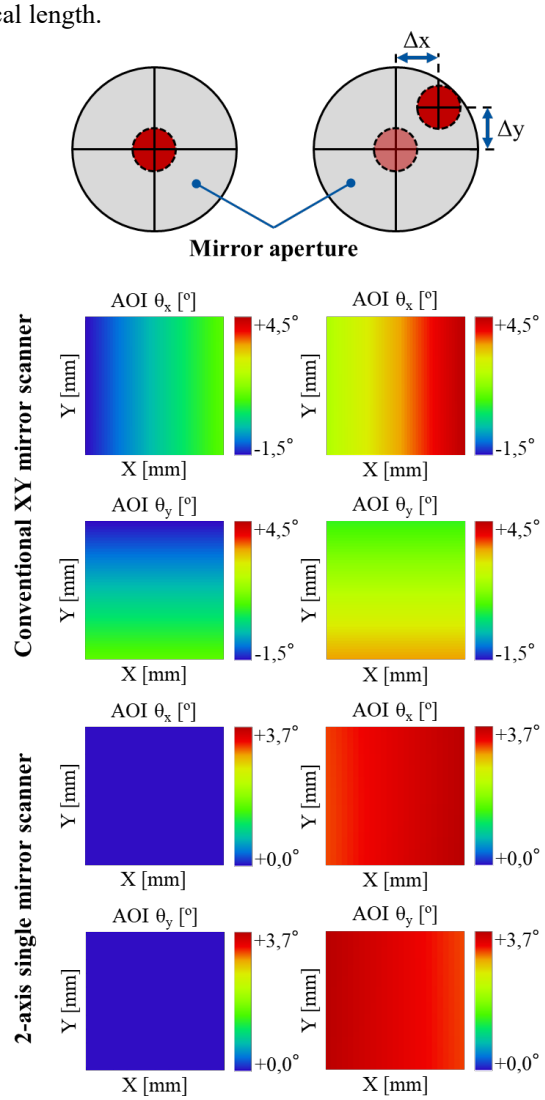

Fig. 7 Simulated AOI for an input beam offset of 3 mm in X and Y as a function of the position in scan field for conventional XY-mirror scanner vs single mirror scanner. The focusing lens is an ideal f-theta objective with a focal length of f = 50 mm. The displayed square scan field has an edge length of 7 mm.

The simulations compared a conventional 2-mirror scanner with a 30 mm aperture to a single-mirror scanner a comparable clear aperture. With the selected aperture size and beam diameter, a maximum beam offset of 3 mm in X and Y within the system can be realized to evaluate performance at extreme positions. By considering these assumptions, the simulations aimed to provide a comprehensive comparison of the realistically achievable AOIs and its robustness across the scan field between the conventional 2-mirror scanner and the single-mirror scanner under realistic operating conditions.

The simulated results are shown in Fig. 7. For both scanner systems, the maximum beam offset of 3 mm results in an average AOI of 3.4°. across the whole scan field. Based on our initial experimental results, this is already sufficient. Considering the telecentric error, the single-mirror scanner system has only a telecentric error of ±0.25° which is significantly smaller of than the system with the conventional scanner. The latter leads to an unacceptable value of ±1.46°. With such a large telecentric error, the AOI might even fall under the absolute limit of 3° from a scan field position of 0.5 mm. It becomes obvious that a single-mirror scanner is much more suitable for scanning an inclined beam.

4. Conclusion

This study has demonstrated the potential of liquid crystal on silicon spatial light modulators in achieving vertical wall angles in ultrashort pulse laser ablation, addressing a significant challenge in precision laser processing. By integrating two cascaded SLMs into the beam path before the scanner, it is possible to manipulate the AOI digitally. Furthermore, the use of SLMs in beam manipulation offers additional advantages such as the capability for superposed beam shaping and splitting.

A series of experiments was conducted to determine the required AOI by varying the fluence and the number of passes. These experiments revealed that the smallest achievable wall angle is 3° when using a fluence of F_0 = 10 J/cm². It was concluded that an AOI of at least the same 3° is necessary for achieving taper-free cuts, with 5° or more being preferable to reduce the required fluence or number of passes.

The phase masks used for beam deflection were evaluated, verifying that shorter grating periods result in larger deflection angles but lower optical efficiency. Conversely, longer grating periods, which maintain high optical efficiency, require a longer distance between the two SLMs to achieve the desired parallel offset of the raw beam. For a beam path as short as possible and an AOI as large as possible, it is advantageous to choose an f-theta lens with the shortest available focal length.

Furthermore, we found that conventional 2-mirror scanners are not suitable for the presented approach due to the relatively large telecentric error which would disturb the intention of a defined constant AOI. The simulation results indicate that a single-mirror scanner cause a negligible telecentric error ideal for scanning inclined beams.

Acknowledgements
This research was funded by the European Union**.**

References

[1] M.N. Polyanskiy: Sci. Data, 11, (2024) 94.
[2] A. Michalowski: "Untersuchungen zur Mikrobearbeitung von Stahl mit ultrakurzen Laserpulsen", (Utz, München, 2014) 39.
[3] D. Haasler and A. Gillner: Proc. SPIE, Vol. 11994, (2022) 119940I.
[4] W. Wawers: "Präzisions-Wendelbohren mit Laserstrahlung", (Shaker, Aachen, 2008) 10.
[5] C. Föhl: "Einsatz ultrakurz gepulster Laserstrahlung zum Präzisionsbohren von Metallen" (Utz, München, 2011) 27.
[6] Aerotech: Five-Axis Precession Scanner AGV5D, https://www.aerotech.com/wp-content/uploads/2021/01/agv5d-1.pdf (accessed 23 June 2024).
[7] Novanta Photonics: PRECESSION ELEPHANT 2, https://novantaphotonics.com/wp-content/uploads/2021/12/datasheet_multi_axis_scan_head_precession_elephant2.pdf (accessed 23 June 2024).
[8] G. Mincuzzi, M. Faucon, and R. Kling: Opt. Lasers Eng., 118, (2019) 52.
[9] J. Auerswald, T.G. A. Ruckli, P. Weber, D. Diego-Vallejo, and H. Schlüter: J. Mech. Eng. Autom., 6, (2016) 334.
[10] R. Braunschweig, P.E. Martin, J.A. Ramos de Campos, A. Kupisiewicz, S. Estival, and M. Dijoux: Proc. SPIE, Vol. 10744, (2018) 107440U.
[11] Hamamatsu Photonics: SLM X15213 series, https://www.hamamatsu.com/content/dam/hamamatsu-photonics/sites/documents/99_SALES_LIBRARY/lpd/x15213_E.pdf (accessed 23 June 2024).
[12] W. Wang, X. Mei, G. Jiang, S. Lei, and C. Yang: Appl. Surf. Sci., 255, (2008) 2303.
[13] C. Rosales-Guzmán: "How to Shape Light with Spatial Light Modulators" (SPIE, Bellingham, 2017) 5.
[14] N. Levichev, P. Herwig, A. Wetzig, and J.R. Duflou: Procedia CIRP, 111, (2022) 746.

(Received: July 25, 2024, Accepted: December 29, 2024)